Fabrication of UO_2-Mo composite fuel with enhanced thermal conductivity from sol-gel feedstock[a]

S.C. Finkeldei*, J.O. Kiggans, R.D. Hunt, A.T. Nelson, K.A. Terrani

Oak Ridge National Laboratory, 1 Bethel Valley Road, Oak Ridge, TN

*corresponding author: finkeldeisc@ornl.gov

Abstract

Fabrication of monolithic UO_2 and UO_2-Mo composites from Mo metal powder feedstock and UO_3 spheres derived from internal gelation was explored. The addition of 10 vol% Mo as a secondary phase to UO_2 led to an increase of up to 30% in thermal conductivity compared to syntheses in which only pure UO_2 was used. Using coarse and fine Mo metal powder feedstock led to different microstructures, influencing the thermal conductivity of the resulting composites.

Keywords: internal gelation, uranium dioxide, enhanced thermal conductivity, molybdenum

1. Introduction

Uranium dioxide is the most commonly used fuel in water-cooled nuclear power plants for electric power production. UO_2 has a robust, well-established fabrication route [1], excellent radiation damage resistance [2], environmental stability in water [3] and steam [4], and a high melting point [5], all of which make it a suitable fuel. Due to an obvious economic driving force,

fuel discharge burnup in light water reactors (LWRs) has consistently increased over the decades, but it has slowed down in recent years [6]. The increasing discharge burnup trend over the decades was facilitated by (1) the use of improved Zr-based cladding with slower oxidation rate and hydrogen pickup fraction [7], (2) increased fresh fuel enrichment and utilization of burnable absorbers, and (3) reduction in fuel pin diameter to limit fuel centerline temperature and fission gas release. With the introduction of accident-tolerant fuel cladding variants [8] that do not suffer from limiting phenomena induced by H pickup, along with the potential for enrichment beyond the arbitrary 5% limit, it is possible once again to achieve higher burnups. However, high-performance fuel pellets are also necessary to facilitate this trend. Specifically, improvements in thermal transport and fission gas retention are targeted. These two performance metrics are interrelated, as the majority of fission gas released from fuel is governed by thermally activated processes.

While there is a separate development track to add solutes to uranium dioxide to retard fission gas mobility [9] without significantly affecting its thermal properties, this paper focuses on the addition of metal precipitates to uranium dioxide to enhance its thermal conductivity. The lower fuel temperatures and thermal gradients resulting from this approach increase the margin to melt, and they also increase stored power in the core [10]. Building on the work of Kim et al. [11], the study discussed in this paper examines the use of sol-gel feedstock during fuel fabrication [12]. Molybdenum was chosen as the metallic precipitate because it balances a high melting point, a high thermal conductivity, and a low thermal neutron absorption cross section [11]. This paper presents the methodology for fabricating UO_2 with and without Mo second phases from UO_3 spheres which were synthesized via an internal sol-gel process. The effects of Mo precipitates on the microstructure and the thermal properties of the pellet are reported.

2. Materials & Methods

2.1 Fabrication routes

The high-performance ceramic fuel pellets were fabricated from a UO_3 feedstock produced by an internal sol-gel process [13]. In addition, two reference pellets (P1&2) were fabricated from a UO_2 powdered feedstock which originated from an ammonium diuranate (ADU) powder feedstock. The steps of the fabrication processes are shown in the fabrication route map in Fig. **1**.

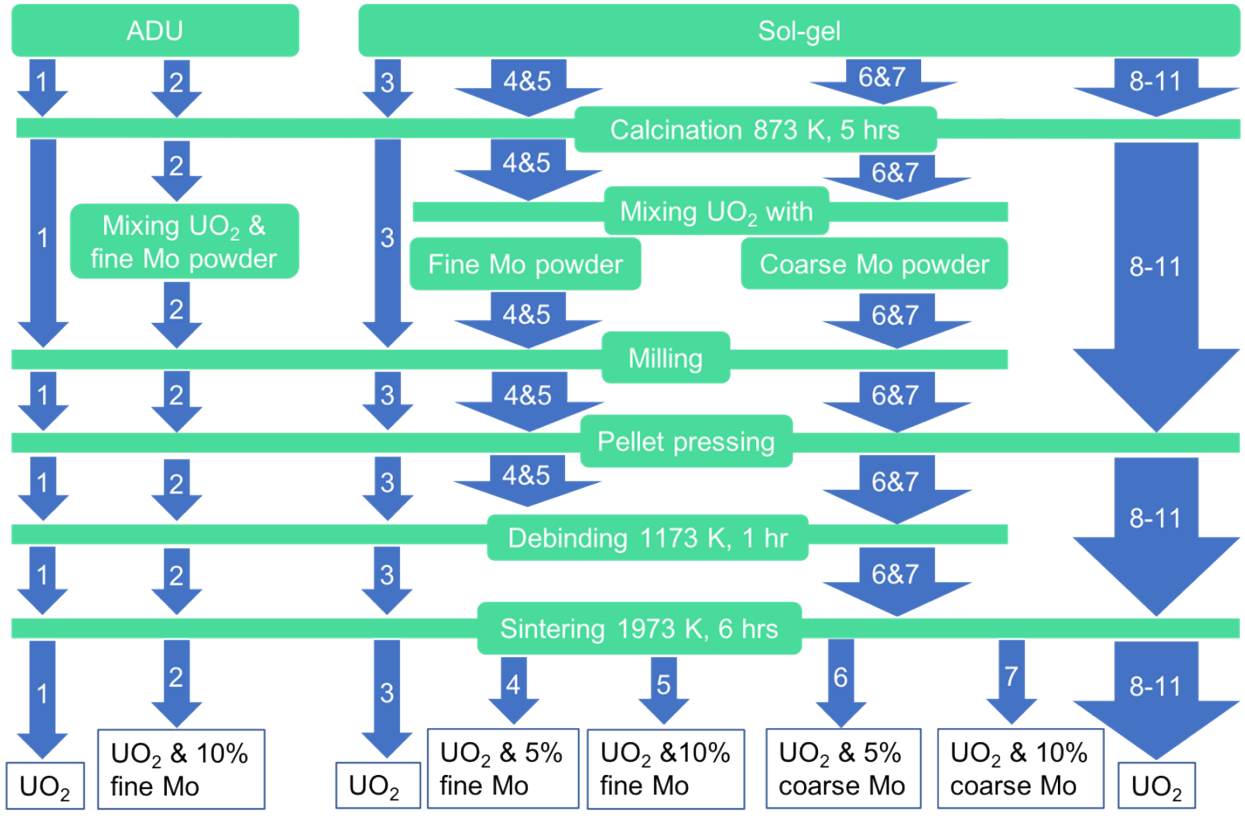

Fig. 1. Fabrication route map for high-performance fuel pellets from two different feedstocks of ADU powder (synthesis routes 1 and 2) and UO_3 microspheres from a sol-gel fabrication route (synthesis routes 3–11). The numbering scheme presented above is used throughout the manuscript to refer to the fabricated pellets via the depicted fabrication route.

2.1.1 Fabrication from an ADU powder starting material

Depleted UO_2 powder from AREVA was recalcined under an Ar-4% H_2 atmosphere. The calcination occurred at 873 K with a 5 h dwell time, with an intermediate dwell time of 30 min at

573 K. For pellet P2, fine Mo powder with 1% Acrawax C as a binder (Lonza, Lot No: C3454285) was mixed with the calcined UO_2 powder in a SpeedMixer (DAC 150.1 V FVZ Remote, FlackTek) for 30 seconds at 650 rpm. The actual amounts are depicted in Table 1 and it was targeted for a 10 vol% Mo content for pellet P2. The pellets were pressed in a 10.2 mm die at 40 MPa for 2 minutes. A UO_2 reference pellet P1, without Mo was pressed under the same conditions. Debinding occurred in a tube furnace under an Ar-4% H_2 atmosphere. The final debinding temperature was 1,173 K with 1 h dwell time, whereas a 30 min dwell time at 573 K and a 1 h dwell time at 903 K occurred during heating. Sintering occurred in an Ar-4% H_2 atmosphere in a tungsten heating element furnace (Materials Research Furnaces, Inc.) at 1,973 K. A heating rate of 3 K/min was applied up to 373 K and was increased to 5 K/min up to 473 K, with a final heating rate of 10 K/min to 1,973 K and a sintering duration of 6 h. The cooling rate was 10 K/min.

Table 1
Amounts of UO_2 and Mo powder for pellet fabrication from a UO_2 powder feedstock.

ID	Nomenclature	M (UO_2 & Acrawax C) (g)	m (Mo) (g)	Vol% Mo (%)	Total pellet mass (g)	Pellet ratio L/D
P1	ADU UO_2	0.4233	-	-	0.4233	0.11
P2	ADU UO_2 10% Mo fine	0.4206	0.0478	10.8	0.4684	0.11

2.1.2 Fabrication from a UO_3 sol-gel microsphere feedstock

A UO_3 microsphere feedstock was fabricated via an internal sol-gel process [13]. Four batches of UO_3 microspheres < 75 μm, 150–212 μm, 212–300 μm, and 300–425 μm were reduced to UO_2 in an Ar-4% H_2 atmosphere. The same calcination conditions as described above were applied. The calcined spheres were the precursors for the pellet fabrication in the experiments described below.

A total of 4 g UO_2 from the < 75 μm batch was mixed for 30 sec with 0.1% Acrawax C as a binder. Subsequent milling for 2 min in a high energy mill (SPEX 8000M Mixer/Miller) with zirconia milling media was repeated three times.

2.1.2.1 UO_2 reference pellet

A reference pellet (P3) was produced using a 0.2230 g charge of milled UO_2 which was biaxially cold pressed in a 10.2 mm die at 200 MPa for 10 seconds. Debinding and sintering occurred as described in section 2.1.1.

2.1.2.2 UO_2 pellets containing 5 vol% and 10 vol% Mo

Molybdenum powder (nanomaterials, particle size <800 nm) referred to as *fine Mo* hereafter, and a mixture of Mo powder (mixing 27 g Climax Mo powder, NPA grade with 95% <63 μm particle size and 73 g TEKMAT Mo-45 powder, 15–45 μm particle size) referred to as *coarse Mo powder*, were used. 1% Acrawax C was added to each Mo starting powder respectively and was mixed for 10 minutes in a ball mill.

UO_2 pellets (P4-7) with 5 vol% and 10 vol% Mo were prepared. The volume percentages of Mo and UO_2 were converted into weight fractions using their theoretical densities. The respective amounts of the calcined UO_2 spheres and the Mo powder (Table 2) were mixed for 30 sec via high speed shaking on a Vortex mixer (Vortex-Genie 2, Scientific Industries). To ensure a thoroughly mixed and homogeneous starting material the mixed UO_2 and Mo were milled for 2 min 3 times in a high energy mill. The blended powders were biaxially pressed in a 10.2 mm die at 200 MPa for 10 sec. The debinding and sintering steps were conducted under the same conditions as described in section 2.1.1.

Table 2.

Sample compositions fabricated from UO_2 microspheres and Mo powder. The volume percentage values for Mo correspond to the actual weighed amounts of Mo and are nominally referred to in the paper as 5 and 10 vol%, respectively. The amounts of UO_2 and Mo given are the actually weighed masses from which multiple pellets were fabricated. Therefore the total pellet mass is lower than the combined weights of UO_2 and Mo.

ID	Nomenclature	m (UO_2) (g)	m (Mo) (g)	Vol% Mo (%)	Total pellet mass (g)	Pellet ratio L/D
P3	Sol-gel UO_2	0.2230	-	-	0.2230	0.27
P4	Sol-gel UO_2 5% Mo fine	3.8742	0.1868 (fine)	4.9	1.3465	0.27
P5	Sol-gel UO_2 10% Mo fine	3.6883	0.3851 (fine)	10.0	1.3355	0.27
P6	Sol-gel UO_2 5% Mo coarse	3.8891	0.1843 (coarse)	4.8	1.3342	0.27
P7	Sol-gel UO_2 10% Mo coarse	3.6974	0.3782 (coarse)	9.8	1.2964	0.27

2.1.2.3 Direct fabrication of UO_2 pellets from sol-gel spheres

The calcined UO_2 spheres were directly mixed and subsequently pressed into pellets (P8-11). The exact compositions are given in

Table **3** and were chosen by taking findings about the packing efficiency regarding mixing ratios and size ratios from the literature [14,15] into account. The calcined UO_2 spheres were mixed for 10 sec on a Vortex mixer at low speed. After loading a 4 mm die, the die was vibrated for 20 sec. For pellet P11, the die was subsequently loaded starting with the biggest spheres and progressing to the smallest spheres, with vibrating steps between each sphere loading step. All pellets were biaxially cold pressed for 2 min at 200 MPa. The pellets were sintered under the same conditions as described in section 2.1.1.

Table 3.

Composition of UO_2 pellets directly fabricated from microspheres, with corresponding sphere sizes of dried UO_3 spheres.

ID	Ratio	Mass (g) <75 μm	Mass (g) 150–212 μm	Mass (g) 212–300 μm	Mass (g) 300–425 μm	Pellet ratio L/D
P8	3:7	0.0398	-	-	00833	0.46
P9	1:1:1	0.0412	-	0.039	0.0397	0.48
P10	67:23:10	0.0147	0.0265	-	0.0792	0.44
P11	67:23:10	0.0118	0.0265	-	0.0792	0.47

2.1.2.4 Direct mixing and pressing of Mo and UO_2 spheres

UO_2 pellets with 5 vol% and 10 vol% Mo were prepared from < 75 μm and 300–425 μm UO_2 spheres. The two size fractions of UO_2 spheres were mixed for 10 sec on a Vortex mixer, and after adding the appropriate Mo amount, they were mixed for 30 sec at 650 rpm. Pellets were pressed at 200 MPa for 10 sec, and the sintering conditions described above were applied. This fabrication led to an inhomogeneous Mo distribution within the pellets, and further enhancement of the fabrication route is planned. Therefore, this fabrication route is not depicted in Fig. **1**.

2.2 Characterization

2.2.1 Thermogravimetric analysis

To identify the starting composition of the precursor UO_3 spheres from the sol-gel fabrication, this material was analyzed by thermal gravimetric (TG) analysis with a simultaneous thermal analyzer (STA) Netzsch 449 F3 Jupiter. The analysis involved placing 165.8 mg of this material in an alumina crucible and heating it at 1 K/min to 1,273 K in an Ar-4% H_2 atmosphere

using a silicon carbide furnace. System calibrations were initially performed to confirm that the target temperature is within 10 K of the actual temperature.

2.2.2 Density determination

The green and sintered densities of the fabricated pellets were determined geometrically. In case of the risk to damage the pellet during handling, the green density was not determined. The height and diameter were measured three times each at each pellet with calipers. The pellet was rotated ~120° in between these measurements and the values here reported are the average values of these three measurements. The theoretical densities (TDs) of composite UO_2-Mo pellets (P2, P4-7) were calculated via the corresponding volume fractions of the crystallographic density ρ_c of Mo (10.280 kg/m^3) and UO_2 (10.970 kg/m^3) [16]:

$$TD = (\text{volume fraction } UO_2) \cdot \rho_c(UO_2) + (\text{volume fraction Mo}) \cdot \rho_c(Mo) \quad (1)$$

2.2.3 Structural characterization

Structural characterization was performed via x-ray diffraction using a D2 Phaser from Bruker with θ-2θ geometry. The instrument uses a Cu k_α source with λ = 1.5406 Å. The step width was 0.004° with a measurement duration of 42.64 seconds per step, and the data were collected from 10–110°. Measurements were performed on the intact pellets, which were encapsulated in Kapton foil.

2.2.4 Microstructural characterization

The microstructural characterization was performed via scanning electron microscopy (SEM) using a FEI VERSA 3D Dual Beam FIB-SEM, in combination with energy dispersive x-ray

spectroscopy (EDS) using an Oxford X-Max150 SDD EDS detector. Image analysis was performed using the Image *J* Image Analysis Suite [17]. The estimated Mo particle sizes were determined from EDS mapping, whereas the pore sizes were extracted from backscattered electron (BSE) images.

2.2.5 Thermal diffusivity and conductivity

Thermal diffusivity α was measured with a Netzsch LFA 457 in an Ar-4% H_2 atmosphere to avoid oxidation in 100 K temperature intervals from 373–1,373 K. Data was collected during both heating and cooling for a subset of samples, and no hysteresis was observed. Only data for heating the sample were considered for the data evaluation reported. The reported thermal diffusivity values were the averaged values of 5 measurements at each temperature. The data were fitted with the Cowan + pulse correction model [18]. To derive the thermal conductivity *k*, the geometrically determined density ρ was used. The thermal expansion was assumed to be dominated by UO_2 [19], and temperature-dependent thermal expansion values from Conway [20] were used to correct for the temperature-dependent densities. The specific heat (c_p) was calculated via mass fraction for each sample, with temperature-dependent literature values for UO_2 [21] and Mo [22]. To allow for comparison of all fabricated fuel candidates, which vary slightly in density, all data were corrected for a 95% TD fuel pellet with the Loeb equation [23] [24] :

$$k(T) = (1 - p) \cdot k_{TD}(T) \quad (2)$$

In compliance with the ASTM Standard [25], a 3% standard error for the thermal diffusivity measurements, in combination with the error of the density and the thermal conductivity, resulted in a standard error of 5% for the thermal conductivity.

3. Results

3.1 Feedstock analysis & fabrication route design

The feedstock analysis as well as an evaluation of the here presented fabrication routes are reported within the next two subsections. Subsequently structural, thermal and microstructural properties of the fuel candidates were studied.

3.1.1 Thermogravimetric analysis of UO_3 feedstock

Thermogravimetric analysis of the as-prepared spheres showed a mass loss in three steps (Fig. **2**). The curve shape is in agreement with the data reported by Eloirdi et al. [26] on an ammonium diuranate sample. They describe the first weight loss step ranging up to 573 K to be caused by the dehydration, followed by a denitration step at around 723 K, and crystallization as UO_3 at around 873 K.

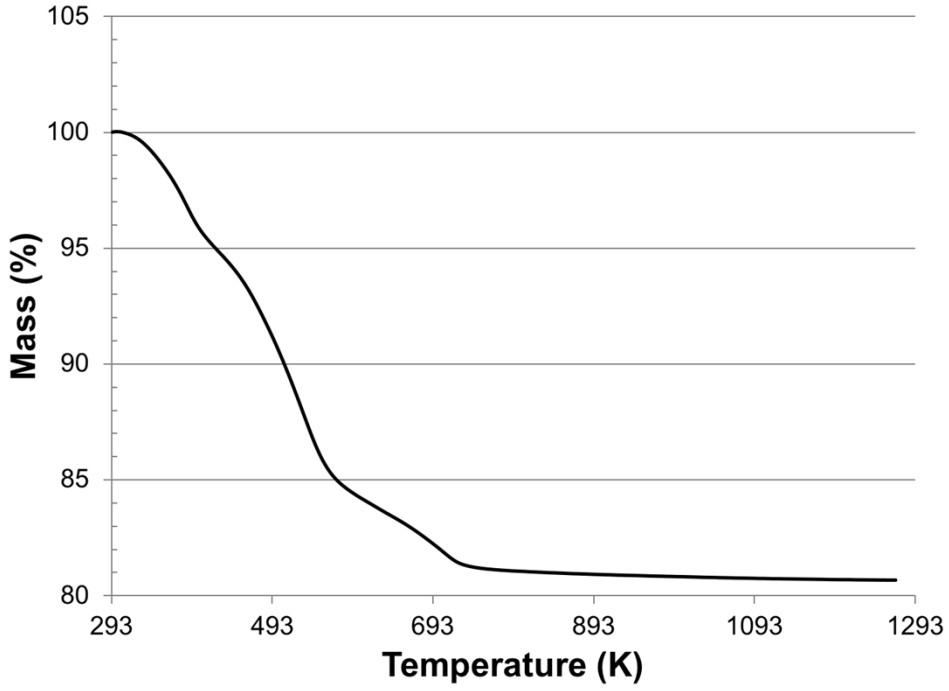

Fig. 2. Thermogravimetric curve of UO_3 spheres as fabricated via the internal sol-gel synthesis. The TG measurement was performed in an Ar-4% H_2 atmosphere.

In this study, a weight loss of 17.10 wt% was determined and is correlated with $3UO_3*NH_3*6H_2O$ as the precursor. The thermogravimetric analysis ensured that the temperature of 873 K was sufficient to remove the attached water and ammonia residuals originating from the sol-gel fabrication process.

3.1.2 Fabrication route design

To enable a comparison of the results from the fabricated pellets used in this study with the results published in the open literature, a UO_2 pellet (P1), as well as a UO_2 pellet with 10 vol% Mo (P2), were prepared from an ADU powder feedstock (pellets P1 and P2, Fig. **1**).

In a first attempt for the microsphere feedstock routes, calcined UO_2 spheres were milled and directly pressed into a pellet as the reference pellet (pellet P3), whereas the calcined UO_2 spheres were mixed with Mo and Acrawax C in the respective amounts (Table 2) to fabricate UO_2 pellets with 5 vol% and 10 vol% Mo (pellets P4-7), respectively. Scanning electron microscopy (SEM) investigations revealed that the Mo powder underwent plastic deformation without experiencing notable size reduction. To avoid crushing the UO_2 spheres and to directly use the UO_2 precursor in sphere form, a fabrication route for nominally pure UO_2 pellets was explored using pellets P8–11. The advantage of such a fabrication route is that there is no dust formation present, which minimizes the incorporation and inhalation risk. This advantage will be of particular interest for mixed oxide (MOX) fuel fabrications [27]. To obtain fuel pellets with high densities, binary and ternary sphere size systems were chosen. Size ratios and packing theories from Del Cul [14] and Ayer [15] were considered; this approach led to the sphere sizes and ratios used in this study. The experimental effort to mix these spheres with fine Mo powder and to directly press pellets resulted in inhomogeneous pellets. No homogeneous dry coating of the UO_2 spheres was observed during the applied mixing process. To evaluate the experimental efforts of the fuel

candidate fabrication processes and the fuel properties, the pellets were structurally and microstructurally characterized, and their thermal conductivity was determined and compared.

3.2 Density characterization

Table **4** shows the geometrically determined densities for the fabricated fuel pellets. The results indicate that there is no direct correlation between the density and the presence of fine or coarse Mo powder as the secondary phase on the green density as well as the sintered density. However, a decreasing trend in sintered densities was observed in relation to the addition of 10 vol% Mo as compared to 5 vol% Mo. Pellets P1 and P2, which were prepared from the ADU powder as starting material, exhibited lower densities at around 90% TD as compared to the pellets prepared from a microsphere feedstock. This was expected due to the lower pressure applied during their preparation. The SEM analysis of the composite fuel pellets (Section 3.5) indicated all porosity should be located within the UO_2 phase. Further analysis of the thermal properties of the composite pellets was based on this assumption.

The direct pelletization of the microspheres into fuel pellets (P8-11) was successful, resulting in densities of around 95% TD except for in pellet P10. The densities presented herein are comparable with the results from Zimmer et al. [28], who used microspheres prepared via an external gelation route with carbon black as the pore former.

Thus, the size ratios of the microspheres and subsequent fabrication routes in Section 2.1.2 provide a suitable fabrication recipe for dense fuel pellets via sol-gel microsphere pelletization (SGMP).

Table 4.

Geometrically determined densities for the prepared fuel candidate pellets. The subscript Mo_f indicates the usage of the finer Mo powder, whereas Mo_c corresponds to the coarser Mo starting material.

ID	Composition	Green density (% TD)	Sintered density (g/cc)	Sintered density (% TD)
P1	ADU UO_2	-	9.9	90.6
P2	ADU UO_2 10 vol% Mo_f	-	9.8	90.2
P3	Sol-gel UO_2	55.4	10.0	91.3
P4	Sol-gel UO_2 5 vol% Mo_f	55.5	10.2	93.6
P5	Sol-gel UO_2 10 vol% Mo_f	53.6	9.9	91.1
P6	Sol-gel UO_2 5 vol% Mo_c	54.9	10.2	93.1
P7	Sol-gel UO_2 10 vol% Mo_c	57.5	9.4	86.1
P8	Sol-gel UO_2 (3:7)	44.1	10.4	94.9
P9	Sol-gel UO_2 (1:1:1)	43.7	10.4	95.0
P10	Sol-gel UO_2 (67:23:10)	45.8	10.1	91.9
P11	Sol-gel UO_2 (67:23:10)	44.8	10.6	96.9

3.3 Structural Characterization

The x-ray diffraction pattern for a reference UO_2 pellet (P3), a 5 and 10 vol% Mo sample (P4&5), were measured. Fig. **3** shows the x-ray diffraction (XRD) pattern for a UO_2-5 vol% Mo fuel pellet (P4). The broad feature at the lower 2Theta values is caused by the Kapton foil in which the pellet was encapsulated during the measurement. As a standard procedure, LaB_6 was added, and the corresponding diffraction peaks are marked with asterisks. The XRD pattern confirmed the formation of a composite fuel pellet. UO_2 crystallized in the cubic fluorite structure. The lattice parameter of the UO_2 phase was determined to be 5.4642 Å ± 0.0002 Å. Separate diffraction peaks were present for Mo, confirming its crystallization in a body-centered cubic structure in the space group Im-3m.

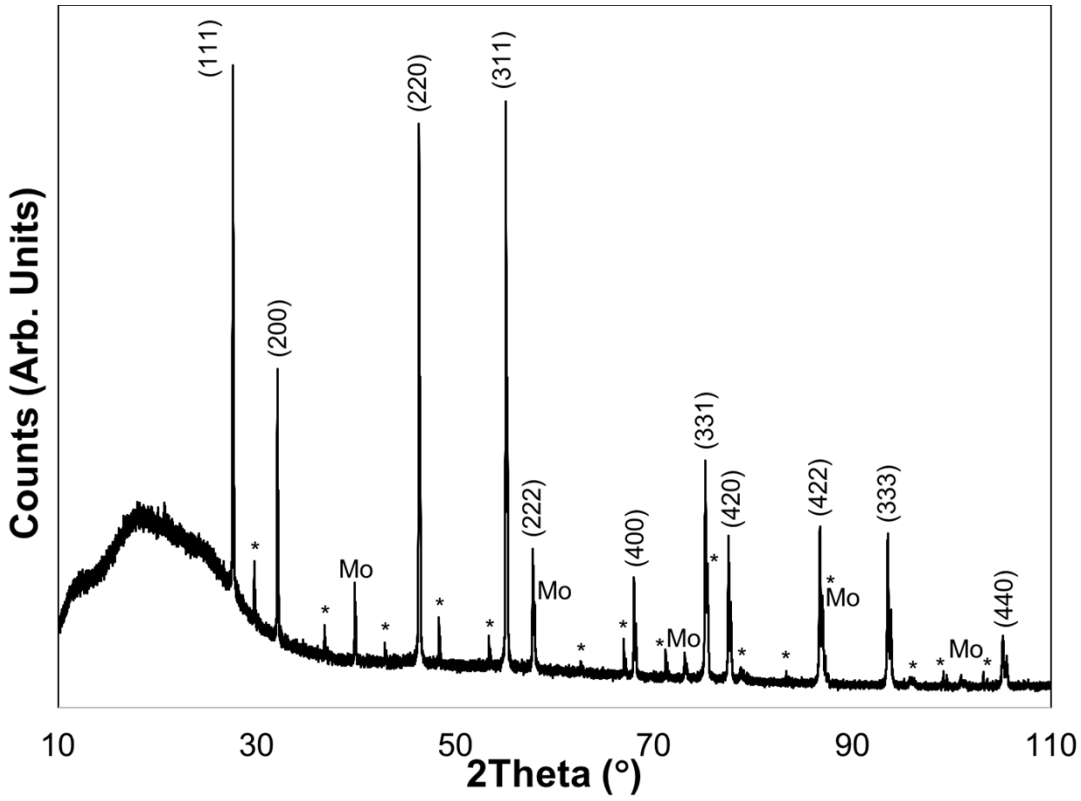

Fig. 3. XRD pattern of a UO_2-5 vol% Mo pellet (P4) showing the formation of a composite fuel of UO_2 with Mo as a secondary phase. The UO_2 diffraction peaks are indexed, and diffraction peaks of the body-centered cubic Mo phase are marked by "Mo." The diffraction peaks of the LaB_6 standard are marked by asterisks *.

3.4 Thermal diffusivity and conductivity

To allow for comparison of all fabricated fuel candidates, all data were corrected for a 95% TD fuel pellet via equation (2), as presented in Section 2.2. Fig. **4** shows the thermal conductivity values for nominally pure UO_2 pellets prepared from a sol-gel feedstock (P3) (solid black circles) and from a powder (P1) (solid red triangles). These data are compared to references of nominally pure UO_2 samples. The references from Fink [29] (orange dotted curve) and White [30] (gray dashed curve) for UO_2 samples show that there is a variation of the thermal conductivity values for pure UO_2 samples. This variation is more pronounced at lower temperatures. The powder used to fabricate the pellet P1, referred to as ADU UO_2 (solid red triangles), originates from the

same batch of UO_2 powder from AREVA that was used to fabricate the pellets measured by White et al. [30]. The thermal conductivity data for these two pellets are in very good agreement between 472–972 K. The pellet prepared from a powder starting material (P1) (ADU, solid red triangles) for this study showed a 13% lower thermal conductivity as compared to the UO_2 pellet (P3) prepared from a sol-gel feedstock (solid black circles). This observation was previously made by Ganguly et al. [31][32], who observed an enhanced thermal conductivity for UO_2 pellets prepared via the direct pelletization of microspheres when compared to UO_2 pellets prepared from a powder precursor.

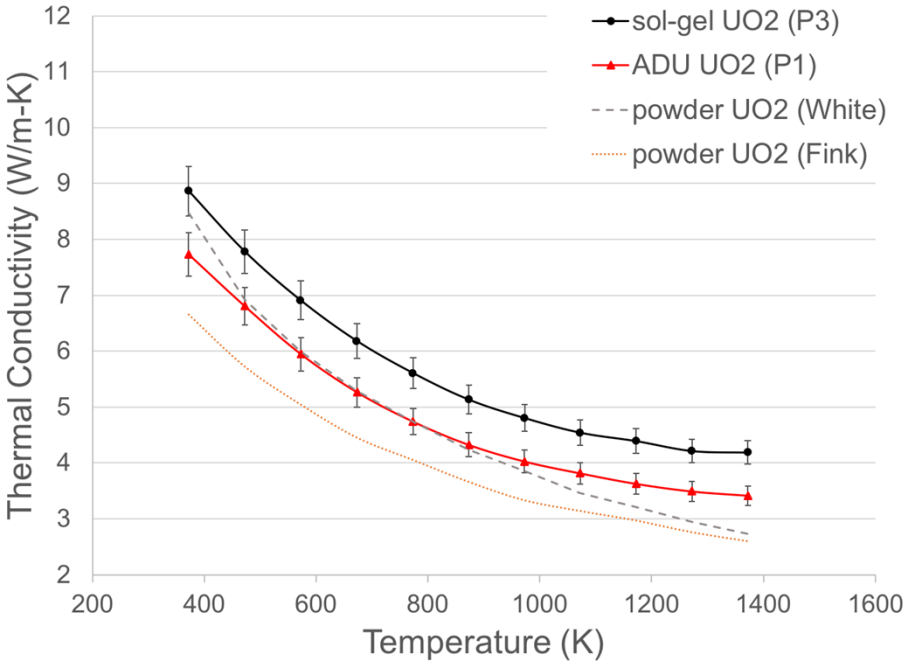

Fig. 4. Temperature-dependent thermal conductivity of UO_2 prepared from a sol-gel feedstock (P3) (solid black circles) and from a powder feedstock (P1) (solid red triangles). Literature values from White (gray dashed curve) and Fink (orange dotted curve) are plotted as a reference for UO_2.

Fig. **5** shows the thermal conductivity for a UO_2 - 5 vol% Mo pellet (P4) (solid green rectangles) compared to the pure UO_2 reference pellet (P3) (solid black circles) both fabricated

from a sol-gel feedstock. The curve of Fink for a pure UO_2 pellet was added as reference data set for all here presented thermal conductivity measurements (orange dotted curve). Moreover, the models for the thermal conductivity for a composite material, depending on the distribution of the secondary phase, are plotted in Fig. **5** and explained below. The expected thermal conductivities for the rule of mixture (dark blue curve, Fig. **5**) according to

$$k_{Mo-UO_2} = V_{UO_2} \cdot k_{UO_2} + V_{Mo} \cdot k_{Mo}, \tag{3}$$

and the inverse rule of mixture (light blue curve, Fig. **5**),

$$\frac{1}{k_{Mo-UO_2}} = \frac{V_{UO_2}}{k_{UO_2}} + \frac{V_{Mo}}{k_{Mo}} \quad , \tag{4}$$

with the thermal conductivity *k* and the volume fraction *V* for the different species, give upper and lower boundary values for the expected thermal conductivity of a composite material [16]. For composite materials with a dispersed phase, which is the case for this study's prepared samples, the bulk conductivity can be approximated by the following equation [16]:

$$k_{Mo-UO_2} = k_{UO_2}\left(\frac{1 + 2V_{Mo}\left(1 - k_{UO_2}/k_{Mo}\right)/\left(2k_{UO_2}/k_{Mo} + 1\right)}{1 - V_{Mo}\left(1 - k_{UO_2}/k_{Mo}\right)/\left(k_{UO_2}/k_{Mo} + 1\right)}\right). \tag{5}$$

This approximation is shown as a dotted gray curve (Fig. **5**). The UO_2 - 5 vol% Mo pellet P4, fabricated for this study is in good agreement with theoretically derived values. To depict the minimum and maximum increase for the thermal conductivity of a composite material, the inverse rule of mixture as well as the rule of mixture for composite materials are also shown as lower and upper boundaries.

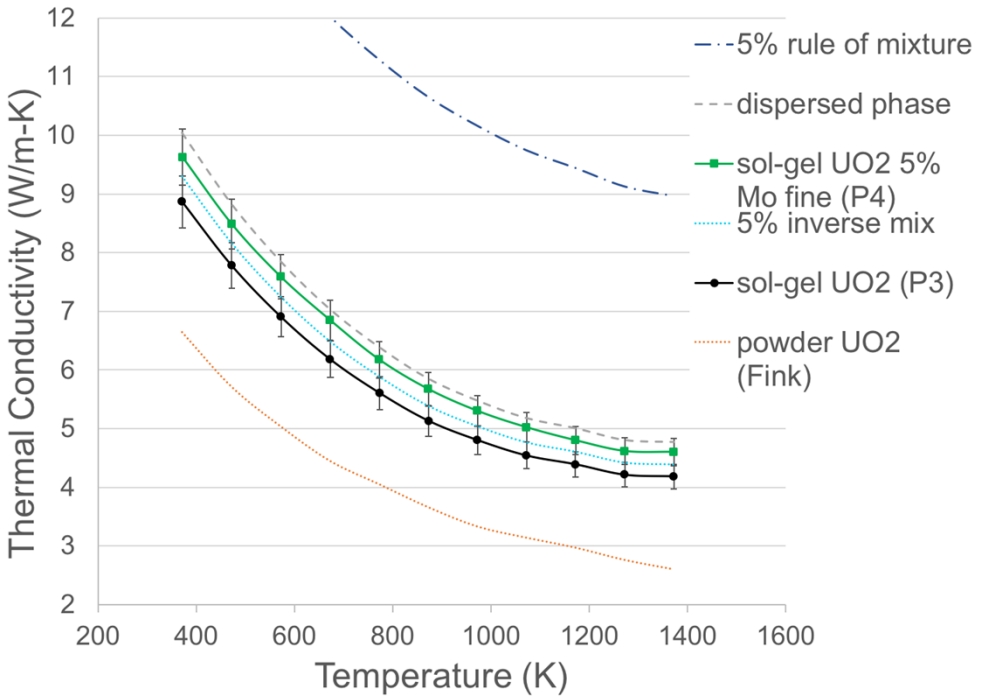

Fig. 5. Temperature-dependent thermal conductivities of UO_2 (P3) (solid black circles) and UO_2 - 5 vol% Mo (P4) (solid green rectangles) fuel candidates compared to theoretically calculated values. The light blue dotted line corresponds to the inverse rule of mixture, the dark blue dash-dotted line indicates the rule of mixture, and the gray dashed line corresponds to the model of a dispersed Mo phase in UO_2. Literature values from Fink (orange dotted curve) are plotted as a reference for UO_2.

A 10% increase in the thermal conductivity is observed for the addition of 5 vol% Mo to UO_2 (P4) as compared to the pure UO_2 pellet (P3) prepared for this study. This is expected as nominally pure Mo has a very high thermal conductivity of 145 W/(m-K) at 290 K [33] which will lead to an increase of the thermal conductivity of the UO_2 - Mo composite fuel candidates.

Fig. **6**a depicts the temperature-dependent thermal conductivity for the pellets fabricated from a powder feedstock (P1 & P2). The addition of 10 vol% fine Mo (P2) (solid green rectangles) to the pellet prepared from a UO_2 powder precursor (P1, *ADU*) (solid red triangles) led to an increase of the thermal conductivity of 8–30% between 372–1,372 K. However, this value is very similar to a pure UO_2 fuel pellet (P3) (solid black circles, Fig. **6**b) prepared from a microsphere feedstock. Fig. **6**b shows the thermal conductivity curves for the UO_2 - 10 vol% Mo pellets (P5 & P7) fabricated from a sol-gel feedstock. The UO_2 - 10 vol% Mo pellet (P7) prepared from a coarse

Mo starting powder (open purple rectangles) showed an increase of 10–20% in thermal conductivity, whereas the fine Mo starting powder (P5) (solid green rectangles) led to a 25–30% increase between 372–1,372 K when compared to the pure UO_2 pellet (P3) from a microsphere feedstock. The model for the inverse rule of mixture (dotted light blue curve) is in good agreement with the coarse UO_2 - Mo pellet (P7) below temperatures of 872 K. The model for a dispersed Mo phase within the continuous UO_2 phase (gray dashed curve) is in good agreement with the fine UO_2 - Mo pellet's (P5) thermal conductivity (solid green rectangles, Fig. **6**b). The thermal conductivity derived via the rule of mixture for UO_2 with 10 vol% Mo drops from 19.7 W/(m*K) at 400 K to 12.2 W/(m*K) at 1,400 K and is far above the values reported here, and it is not plotted in Fig. **6**.

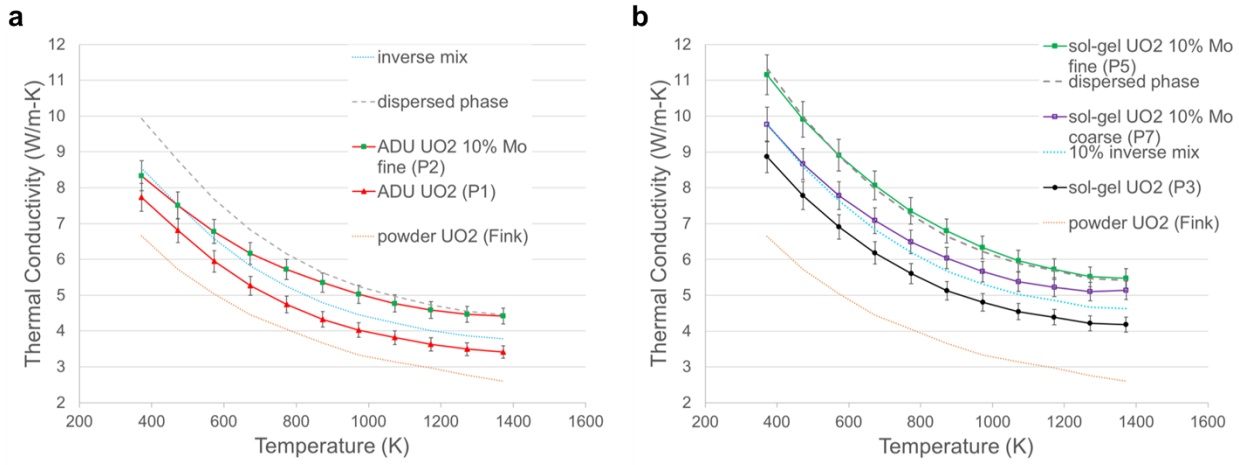

Fig. 6. (a) Temperature dependent thermal conductivity of a pure UO_2 pellet (P1) fabricated from a powder feedstock (solid red triangles), a UO_2 - 10 vol% Mo pellet (P2) fabricated with a fine Mo starting powder (solid green rectangles), as well as the thermal conductivity models for an inverse mix (dotted light blue curve) and for a dispersed phase (gray dotted curve). Literature values from Fink (orange dotted curve) are plotted as a reference for UO_2 in both figures. (b) Temperature-dependent thermal conductivity of a pure UO_2 pellet (P3) (solid black circles), a UO_2 - 10 vol% Mo pellet (P7) fabricated with a coarse Mo starting powder (open purple rectangles), and a fine Mo starting powder (P5) (solid green rectangles), as well as the thermal conductivity models for an inverse mix (dotted light blue curve) and for a dispersed phase (gray dotted curve). All three samples for this plot (b) (P3, P5, P7) were fabricated from a sol-gel UO_3 feedstock.

3.5 Microstructural analysis

The overall microstructure of the fabricated UO_2-Mo pellets was analyzed via SEM. Fig. **7**a and 7c present an overview of the UO_2 - 10 vol% Mo pellets with fine (P5) and coarse Mo (P7) as starting material, respectively. The average particle diameter size of Mo precipitates was determined via the particle analysis tool in Image *J* after creating a binary image with the threshold adjustment. The particle area, derived from this binary image was used to derive the average Mo particle size, assuming spherical particles. The average particle diameter size of the Mo precipitates within these samples are 5.4 μm (P5) versus 29 μm (P7), whereas the UO_2 grain sizes are 8.9 ± 2.9 μm (P5) versus 9.8 ± 2.1 μm (P7) in the corresponding pellets. Uranium dioxide grain sizes were determined via the line intercept method. To gain a better understanding of the pellets' microstructure, the porosity was analyzed via Image *J* and is depicted in Fig. **7**b and 7d for the fine (P5) and coarse (P7) Mo powders, respectively. The average pore size area for the fine UO_2 - Mo pellet (P5) was 0.46 μm^2, where the pore areas ranged between 0.013–77 μm^2. For the coarse UO_2 - Mo pellet (P7), the pore size area ranged between 0.013–174 μm^2, with an average pore size area of 0.93 μm^2. The average pore size area for the coarse Mo powder to fabricate the UO_2 - Mo composite fuel pellets was almost twice as large as for the fine Mo starting powder. The density measurements given in Section 3.2 reveal a density variation of 5% TD between these two samples, with the coarse UO_2 - Mo pellet having the lower overall density. For the thermal conductivity measurements, all values were normalized to 95% TD pellets. The observed lower thermal conductivity for the pellet with the coarse Mo secondary phase (P7) is believed to be caused by the different microstructure of these two fuel candidates.

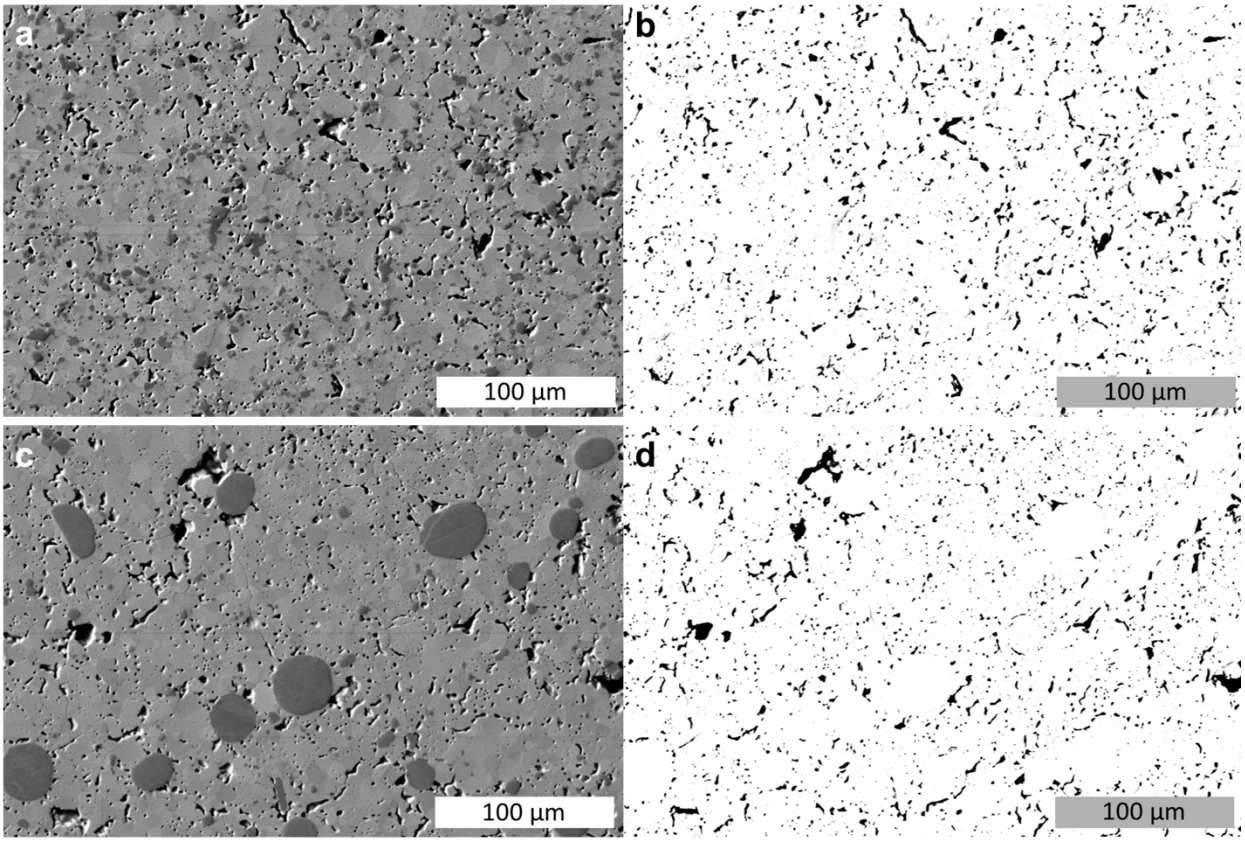

Fig. 7. SEM image of a UO_2 - 10 vol% Mo pellet surface for (a) the fine Mo powder (P5) and (c) the coarse Mo powder (P7). Images b and d show the porosity analysis performed with image J for the fuel pellets with the fine (P5) and coarse (P7) Mo powder, respectively.

Fig 8a shows the calcined UO_2 spheres of the size fraction <75 µm. These spheres were used together with other size fractions (

Table **3**) to fabricate UO_2 pellets (P8 – 11) by directly utilizing the spherical precursor. The fabricated pellets showed a well sintered, dense microstructure (Fig 8b), and densities up to 97% TD were achieved. The microstructural image in Fig 8b is representative of the pellet's surface area.

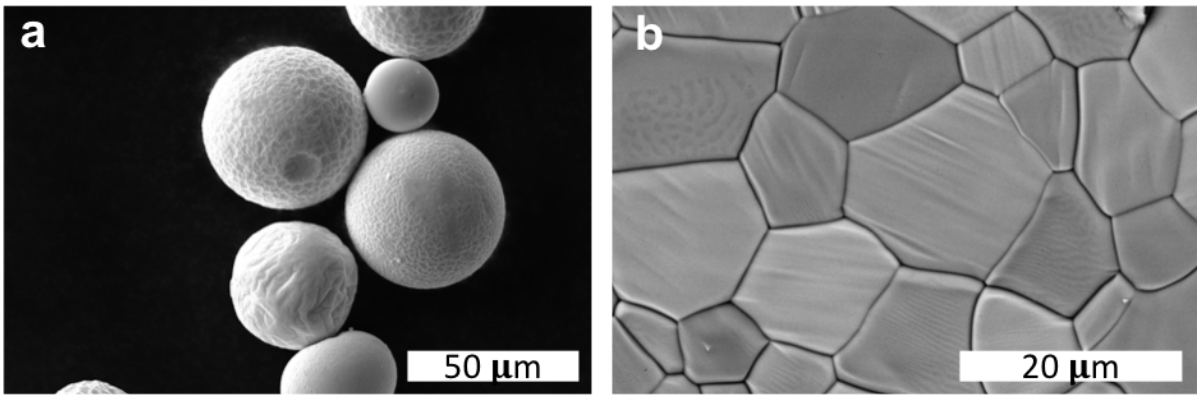

Fig 8. (a) SEM images of the calcined spheres < 75 μm and the pellet prepared for this study and (b) for a nominally pure UO_2 pellet.

4. Discussion

To develop new accident-tolerant as well as high performance nuclear fuels, advanced UO_2 fuels are required in current and future nuclear reactor applications. Two concepts are under consideration for advanced UO_2: (1) addition of dopants to UO_2, and (2) addition of metal precipitates to UO_2. For addition of dopants, Cr, Ti, Mn, and V are considered, along with some other elements. Their addition leads to an enhanced grain growth which is expected to slow down fission product release rates [9]. For the addition of metal precipitates to UO_2, a metal phase is added to UO_2 to increase the overall thermal conductivity of the enhanced UO_2 fuel. Lower temperatures also limit fission product mobility and may reduce release during normal operation. The challenge of adding an inert, non-uranium–bearing phase will result in the loss of ^{235}U unless enrichment is increased.

This study focused on the latter approach, addition of molybdenum to UO_2 with an objective of increasing thermal conductivity. Al, W, Si, Mo, and Zr have been considered, along

with many other compounds, to serve as a secondary phase with a similar purpose [11][34][35]. Molybdenum was chosen as the secondary phase in this study because it has a high melting point, a high thermal conductivity, and a low thermal neutron absorption cross section [11]. In this effort, a UO_3 microsphere feedstock was used to fabricate fuel candidates and enhance the fuel's thermal conductivity. For comparison, two pellets were fabricated from conventional UO_2 powder feedstock (P1 and P2,

Table **4**). The benefits of the fabrication route via a sol-gel fabrication as implemented in this study result from dust minimization during the microsphere syntheses. This is of particular interest for the fabrication of Pu-containing fuel such as MOX, or other transuranic fuel [36][37]. Moreover, the internal gelation efforts underway at the Oak Ridge National Laboratory allow for homogeneous incorporation of other elements besides Pu, such as burnable absorbers by direct addition to the starting broth in the form of a mixable solution or as fine particles [13]. The fabrication route (Fig. ***1***) used in this study for sol-gel derived precursors led to densities of the sintered UO_2-Mo pellets that are comparable to the pellets prepared from UO_2 granules and fine Mo powder by Kim et al. [11]. The pure UO_2 (P3) and the UO_2-Mo pellets (P4-7) fabricated from sol-gel precursors showed an enhanced thermal conductivity when compared to pellets prepared from powder (P1 and P2) (Fig. **4**, Fig. **6**). This is also the case when thermal conductivity values are compared to those obtained from pellets prepared from powder feedstocks as described in the open literature as previously reported by Ganguly et al. [31][32]. They observed an enhanced thermal conductivity for UO_2 pellets that were prepared via the direct pelletization of microspheres when compared to UO_2 pellets prepared from a powder precursor. They attributed the enhanced thermal conductivity to a highly homogeneous distribution of spherical 1.5–3.0 μm pores for the pellets fabricated via the direct pelletization of microspheres.

Even though the secondary phase of metallic Mo obtained in this effort is dispersed within the UO_2 phase (P4-7), a large increase in the thermal conductivity compared to nominally pure UO_2 (P3) is observed. Kim et al. [11] reported a strong increase in the thermal conductivity for a continuous secondary phase of Mo when compared to a dispersed phase of Mo. However, their thermal conductivity for the continuous secondary phase of 10 vol% Mo in UO_2 drops from 9.1 W/(m*K) at 473 K to 3.6 W/(m*K) at 1373 K which is lower than the here reported thermal conductivity values for temperatures below 773 K. At 1,072 K, Kim et al. report a thermal conductivity of 6 W/(m*K) for their continuous Mo phase in UO_2, which is identical to the present

study's value for a UO_2 - 10 vol% Mo pellet (P5) prepared from a fine Mo powder and a microsphere UO_2 feedstock. Yang et al. [38] reported an 80% increase in the thermal conductivity for a continuous phase and 35% for a dispersed phase of Tungsten (W) in a UO_2 - 6 vol% W pellet, respectively. Tungsten has an even higher thermal conductivity [39] than Mo, so it results in a higher percentage increase in the thermal conductivity when compared to the UO_2 - Mo pellets (P4-7) fabricated for this study. However, the fabrication of fuel pellet candidates from microsphere precursors led to a higher thermal conductivity when compared to pellets prepared from powder feedstocks, even though the fuel pellets fabricated for this study exhibit a dispersed secondary phase of Mo rather than a continuous phase of the metal, as was the case for Kim et al. [11]. The microstructural analysis of the UO_2 – 10 vol% Mo pellets (P5 and P7) revealed that the pore size of the coarse Mo powder was greater than the pore size of the fine Mo powder by a factor of two. The UO_2 grain size was not affected by the different Mo powder sizes that were added to the UO_2 fuel candidates. It is beyond the scope of this study to determine whether the pore size and porosity distribution inside the pellets or the dopant size played a more dominant role for the thermal properties of these fuel candidates, so additional experimental studies are needed. Moreover, complementary computational studies such as the finite element model of Williams et al. [40] regarding microstructural models of the thermal conductivity of dispersion type fuels may help to define the individual microstructural contributions to the enhanced thermal conductivity of the UO_2 - Mo fuel candidates developed in this effort. Fabrication processes that directly use the UO_2 microspheres without milling steps led to highly dense UO_2 pellets (P8-11) of up to 97% TD (

Table **4**). The relatively rough surfaces of the spheres themselves (Fig 8a) may be advantageous when coating the spheres with Mo or other elements for secondary phase formations. Future work will focus on the direct pelletization of such coated spheres, as it is likely to result in the formation of a continuous secondary phase similar to the microcell concept.

5. Conclusions

This study used UO_3 spheres developed from a sol-gel fabrication route for the first time to fabricate UO_2 - Mo composite fuel candidates. The UO_2 – 10 vol% Mo pellets fabricated for this study showed thermal conductivities enhanced by up to 30% when compared to nominally pure UO_2 pellets that were prepared from a microsphere feedstock. The absolute values are in agreement with thermal conductivities for the UO_2 - Mo microcell pellets from Kim et al. [11], with a continuous secondary phase of Mo enveloping UO_2. The successful fabrication of pellets through direct use of the UO_2 microsphere feedstock is expected to lead to the fabrication of UO_2 - Mo composite pellets with a continuous Mo phase via coating of the spheres.

Acknowledgments

This work was supported by the US Department of Energy Office of Nuclear Energy (DOE-NE) Advanced Fuels Campaign (AFC). The authors would like to thank Stephanie Curlin for LFA measurements, N. Cinbiz and T. Watkins for in-depth discussions, C. Silva for x-ray diffraction measurements, J. McMurray for simultaneous thermal analysis (STA) measurements, and J. Dyer for polishing selected pellets.

Data Availability Statement

The raw/processed data required to reproduce these findings cannot be shared at this time due to technical or time limitations.

6. References

[1] T.R.G. Kutty, P. V Hegde, K.B. Khan, U. Basak, S.N. Pillai, A.K. Sengupta, G.C. Jain, S. Majumdar, H.S. Kamath, D.S.C. Purushotham, Densification behaviour of UO2 in six different atmospheres, J. Nucl. Mater. 305 (2002) 159–168. doi:https://doi.org/10.1016/S0022-3115(02)00934-0.

[2] H. Matzke, P.G. Lucuta, T. Wiss, Swift heavy ion and fission damage effects in UO2, Nucl. Instruments Methods Phys. Res. B. 166–167 (2000) 920–926.

[3] B.J. Lewis, R.D. MacDonald, N. V Ivanoff, F.C. Iglesias, Fuel performance and fission product release studies for defected fuel elements, Nucl. Technol. 103 (1993) 220–245.

[4] D.R. Olander, Y.S. Kim, W.-E. Wang, S.K. Yagnik, Steam oxidation of fuel in defective LWR rods, J. Nucl. Mater. 270 (1999) 11–20.

[5] P. Hofmann, Current knowledge on core degradation phenomena, a review, J. Nucl. Mater. 270 (1999) 194–211.

[6] U.S. Energy Information Adminstration, “Annual commercial spent fuel discharges and burnup, 1968 - June 30, 2013,” (2015).

[7] A. Couet, A.T. Motta, R.J. Comstock, Hydrogen pickup measurements in zirconium alloys: Relation to oxidation kinetics, J. Nucl. Mater. 451 (2014) 1–13.

[8] K.A. Terrani, Accident tolerant fuel cladding development: Promise, status, and challenges, J. Nucl. Mater. 501 (2018) 13–30. doi:https://doi.org/10.1016/j.jnucmat.2017.12.043.

[9] M.W.D. Cooper, C.R. Stanek, D.A. Andersson, The role of dopant charge state on defect chemistry and grain growth of doped UO2, Acta Mater. 150 (2018) 403–413. doi:https://doi.org/10.1016/j.actamat.2018.02.020.

[10] K.A. Terrani, D. Wang, L.J. Ott, R.O. Montgomery, The effect of fuel thermal conductivity on the behavior of LWR cores during loss-of-coolant accidents, J. Nucl. Mater. 448 (2014) 512–519. doi:https://doi.org/10.1016/j.jnucmat.2013.09.051.

[11] D.-J. Kim, Y.W. Rhee, J.H. Kim, K.S. Kim, J.S. Oh, J.H. Yang, Y.-H. Koo, K.-W. Song, Fabrication of micro-cell UO2–Mo pellet with enhanced thermal conductivity, J. Nucl. Mater. 462 (2015) 289–295. doi:http://dx.doi.org/10.1016/j.jnucmat.2015.04.003.

[12] R.D. Hunt, J.L. Collins, M.H. Lloyd, S.C. Finkeldei, Production of more ideal uranium trioxide microspheres for the sol-gel microsphere pelletization process without the use of carbon, J. Nucl. Mater. 515 (2019) 107–110.

[13] R.D. Hunt, J.L. Collins, Uranium kernel formation via internal gelation, Radiochim. Acta. 92 (2004) 909. doi:10.1524/ract.92.12.909.55110.

[14] G.D. Del Cul, C.H. Mattus, A.S. Icenhour, L.K. Felker, D.F. Williams, Fuel Fabrication Development for the Surrogate Sphere-Pac Rodlet, Oak Ridge, 2005. doi:ORNL/TM-2005/108.

[15] J.E. Ayer, F.E. Soppet, Vibratory Compaction: I, Compaction of Spherical Shapes, J. Am. Ceram. Soc. 48 (2006) 180–183. doi:doi:10.1111/j.1151-2916.1965.tb14708.x.

[16] D.W. Richerson, Modern Ceramic Engineering Properties, Processing, and Use in Design, Second Edi, Marcel Dekker, INC., New York, 1992.

[17] C.A. Schneider, W.S. Rasband, K.W. Eliceiri, NIH Image to ImageJ: 25 years of image analysis, Nat. Methods. 9 (2012) 671. http://dx.doi.org/10.1038/nmeth.2089.

[18] R.D. Cowan, Pulse Method of Measuring Thermal Diffusivity at High Temperatures, J. Appl. Phys. 34 (1963) 926–927. doi:10.1063/1.1729564.

[19] S.-H. Kim, C.-Y. Joung, H.-S. Kim, Y.-W. Lee, H.-J. Ryu, D.-S. Sohn, D.-J. Kim, Fabrication method and thermal conductivity assessment of molybdenum-precipitated uranium dioxide pellets, J. Nucl. Mater. 352 (2006) 151–156. doi:https://doi.org/10.1016/j.jnucmat.2006.02.049.

[20] J.B. Conway, R.M. Fincel, R.A. Hein, The Thermal Expansion And Heat Capacity of UO2 to 2200 C, Trans Am Nucl Soc. 6 (1963) 153.

[21] G.E. Moore, K.K. Kelley, High-Temperature Heat Contents Of Uranium, Uranium Oxide,

And Uranium Trioxide, J. Am. Chem. Soc. 69 (1947) 2105–7.

[22] G.W. Lehman, Thermal Properties of Refractory Materials, Ohio, 1960. doi:WADD-TR-60-581.

[23] A.L. Loeb, Thermal Conductivity: VIII, A Theory of Thermal Conductivity of Porous Materials, J. Am. Ceram. Soc. 37 (1954) 96–99. doi:10.1111/j.1551-2916.1954.tb20107.x.

[24] J. Francl, W.D. Kingery, Thermal Conductivity: IX, Experimental Investigation of Effect of Porosity on Thermal Conductivity, J. Am. Ceram. Soc. 37 (1954) 99–107. doi:10.1111/j.1551-2916.1954.tb20108.x.

[25] ASTM Standard Designation: E1461, 2013 “Standard Test Method for Thermal Diffusivity by the Flash Method,” (2013).

[26] R. Eloirdi, D. Ho Mer Lin, K. Mayer, R. Caciuffo, T. Fanghänel, Investigation of ammonium diuranate calcination with high-temperature X-ray diffraction, J. Mater. Sci. 49 (2014) 8436–8443. doi:10.1007/s10853-014-8553-0.

[27] N. Kumar, R. V Pai, J.K. Joshi, S.K. Mukerjee, V.N. Vaidya, V. Venugopal, Preparation of (U,Pu)O2 pellets through sol–gel microsphere pelletization technique, J. Nucl. Mater. 359 (2006) 69–79. doi:https://doi.org/10.1016/j.jnucmat.2006.07.018.

[28] E. Zimmer, C. Ganguly, J. Borchardt, H. Langen, SGMP — an advanced method for fabrication of UO2 and mox fuel pellets, J. Nucl. Mater. 152 (1988) 169–177. doi:https://doi.org/10.1016/0022-3115(88)90323-6.

[29] J.K. Fink, Thermophysical properties of uranium dioxide, J. Nucl. Mater. 279 (2000) 1–18. doi:10.1016/S0022-3115(99)00273-1.

[30] J.T. White, A.T. Nelson, Thermal conductivity of UO2+x and U4O9−y, J. Nucl. Mater. 443 (2013) 342–350. doi:https://doi.org/10.1016/j.jnucmat.2013.07.063.

[31] C. Ganguly, U. Basak, Fabrication of high density UO2 fuel pellets involving sol-gel microsphere pelletisation and low temperature sintering, J. Nucl. Mater. 178 (1991) 179–

183. doi:https://doi.org/10.1016/0022-3115(91)90384-J.

[32] C. Ganguly, Sol-gel microsphere pelletization: A powder-free advanced process for fabrication of ceramic nuclear fuel pellets, Bull. Mater. Sci. 16 (1993) 509–522. doi:10.1007/BF02757652.

[33] T. Barratt, Thermal and Electrical Conductivities of Some of the Rarer Metals and Alloys, Proc. Phys. Soc. London. 26 (1913) 347–371.

[34] M. V Krishnaiah, G. Seenivasan, P. Srirama Murti, C.K. Mathews, Thermal conductivity of selected cermet materials, J. Alloys Compd. 353 (2003) 315–321. doi:https://doi.org/10.1016/S0925-8388(02)01326-9.

[35] S. Yeo, E. Mckenna, R. Baney, G. Subhash, J. Tulenko, Enhanced thermal conductivity of uranium dioxide–silicon carbide composite fuel pellets prepared by Spark Plasma Sintering (SPS), J. Nucl. Mater. 433 (2013) 66–73. doi:https://doi.org/10.1016/j.jnucmat.2012.09.015.

[36] R.D. Hunt, J.L. Collins, T.J. Reif, B.S. Cowell, J.A. Johnson, Key process parameters to modify the porosity of cerium dioxide microspheres formed in the internal gelation process, J. Nucl. Mater. 495 (2017) 33–37. doi:https://doi.org/10.1016/j.jnucmat.2017.08.007.

[37] R.D. Hunt, J.D. Hunn, J.F. Birdwell, T.B. Lindemer, J.L. Collins, The addition of silicon carbide to surrogate nuclear fuel kernels made by the internal gelation process, J. Nucl. Mater. 401 (2011) 55–59. doi:10.1016/j.jnucmat.2010.03.018.

[38] J.H. Yang, K.W. Song, K.S. Kim, Y.H. Jung, A fabrication technique for a UO2 pellet consisting of UO2 grains and a continuous W channel on the grain boundary, J. Nucl. Mater. 353 (2006) 202–208. doi:10.1016/j.jnucmat.2006.01.019.

[39] I. Langmuir, J.B. Taylor, The Heat Conductivity of Tungsten and the Cooling Effects of Leads upon Filaments at Low Temperatures, Phys. Rev. 50 (1936) 68–87. doi:10.1103/PhysRev.50.68.

[40] A.F. Willimas, B.W. Leitch, N. Wang, A Microstructural Model of the Thermal Conductivity of Dispersion Type Fuels with a Fuel Matrix Interaction Layer, Nucl. Eng. Technol. 45 (2013) 839–846. doi:https://doi.org/10.5516/NET.07.2013.714.